

Article

A Sensitivity Analysis of Ship–Bridge Spacing under the Coupling Effect of Turbulence and Ship Motion

Yasi Ye ^{1,2}, Xiaoping Liu ^{1,*}, Yukang Ye ¹, Anbin Li ^{3,4}, Jiaqiang Zhang ¹ and Qijiang Ren ²

¹ School of Hydraulic and Environmental Engineering, Changsha University of Science and Technology, Changsha 410114, China

² Hunan Provincial Communications Planning Survey & Design Institute, Changsha 410200, China

³ Key Laboratory of Agricultural Soil and Water Engineering in Arid and Semiarid Areas, Ministry of Education, Northwest A&F University, Xianyang 712100, China

⁴ Department of Civil and Environmental Engineering, University of Auckland, Auckland 1023, New Zealand

* Correspondence: lxplyt@163.com

Abstract: The hydrodynamics of the flow around piers affects the motion of ships navigating near these structures, while the motion of the ships, in turn, affects the distribution of the flow field near the piers. This study investigates the forces exerted on a ship in various ship–pier transverse distances using commercial computational fluid dynamics (CFD) software, Fluent 13.0, based on the RNG k - ϵ model, complemented by experiments with a physical model. The interaction between the ship’s motion and the flow field near the piers was considered. The results indicate that during the encounter between the ship and the pier, the boundary of the approaching ship affects the flow field near the pier, thereby affecting the generation and detachment of vortices behind the pier. The yaw moment of the ship demonstrates a marked “positive peak–negative peak–positive peak” pattern. Moreover, as the ship–pier transverse distance increases, the impact of the pier on the ship’s motion decreases, and it becomes negligible when the distance reaches 0.9 times the diameter of the pier (D), suggesting that the pier has a minimal impact on ship navigation if the ship–pier transverse distance exceeds this threshold.

Keywords: flow around a cylindrical pier; yaw moment; numerical model; computational fluid dynamics



Citation: Ye, Y.; Liu, X.; Ye, Y.; Li, A.; Zhang, J.; Ren, Q. A Sensitivity Analysis of Ship–Bridge Spacing under the Coupling Effect of Turbulence and Ship Motion. *J. Mar. Sci. Eng.* **2024**, *12*, 1308. <https://doi.org/10.3390/jmse12081308>

Academic Editor: Decheng Wan

Received: 7 June 2024

Revised: 1 August 2024

Accepted: 1 August 2024

Published: 2 August 2024



Copyright: © 2024 by the authors. Licensee MDPI, Basel, Switzerland. This article is an open access article distributed under the terms and conditions of the Creative Commons Attribution (CC BY) license (<https://creativecommons.org/licenses/by/4.0/>).

1. Introduction

The arrangement of piers changes the original flow conditions of rivers and forms a special flow near bridges, which directly affects the motion pattern of passing ships. In particular, a turbulent flow field around piers can easily cause ships to deviate from their courses, endangering their safe navigation through areas near bridges. The turbulent flow field around piers has been investigated, and a few methods for indirectly determining the safe distance between piers and the waterway boundary have been proposed for ship navigation safety [1–5]. However, in a flow field around a solid body, when another object approaches (e.g., encounters with high-speed trains, encounters with ships, and ships passing through piers), the basic properties of this flow field will change. The separation of the shear layers on both sides of the pier as well as the generation and shedding of vortices behind the pier can cause the flow around the pier to be highly turbulent, and these properties are closely related to the relative position of two piers. When a ship approaches or leaves a pier, these properties will be affected and become even more complex [6–8]. For ships, the turbulent flow around a pier can change their hydrodynamic conditions.

Within the hydrodynamics of ships, the prediction of unsteady hydrodynamics around a moving ship is crucial, especially the hydrodynamics of ships in the case of overtaking, meeting, and approaching [9–11]. Tuck and Newman [12] proposed the thin body theory in a two-dimensional flow and the slender body theory in deep and shallow water for calculating ship–ship interactions, which laid a theoretical foundation for subsequent

studies. Kijima [13] applied the slender body theory to numerically simulate the inter-ship hydrodynamics when one ship overtakes another and the behaviors of the two ships near circular and elliptical piers. With the development of computational fluid dynamics (CFD) and the application of particle image velocimetry (PIV) technology to transient, non-contact testing of the flow field in circulating water tanks, more comprehensive studies have been conducted on the mechanism of the interactions between ships. Accurate velocity field and pressure field distributions around a ship body can be obtained through both experiments and numerical simulations [14,15]. The field of ship hydrodynamics has seen rapid advancements. For example, based on the slender body theory, Xu et al. [16] took a pier as a stationary ship, utilized a general model for the hydrodynamic interference between ships to calculate the ship–pier interference hydrodynamics when the ship passed the pier while going in the X direction, and employed the MMG (Mathematical Modeling Group) model to calculate the ship’s maneuverability. By using Fluent 13.0 in CFD software, Gan et al. [17] applied quasi-steady and unsteady numerical methods to simulate the viscous flow field of a ship sailing straight near a pier and then calculated the changes in the disturbance hydrodynamics of the pier for the ship with the ship–pier transverse distance. With overlapping mesh technology, Li et al. [7] simulated the entire process of a ship passing through a pier and monitored the changes in the transverse force, longitudinal force, and yaw moment, as well as the rolling moment. In terms of research using physical models, some scholars have analyzed the interaction between the flow structure around a pier and a ship by measuring the surface pressure, transverse force, and yaw moment of the ship [18–24].

Through testing on physical models, this study observes and analyzes the changing pattern of the yaw moment as a ship passes a pier, utilizes the CFD method to numerically simulate the viscous flow field with unsteady ship–pier hydrodynamic interactions, and employs dynamic mesh technology and the user-defined function (UDF) in Fluent to obtain the fluid–structure interactions between the flow around the pier and ship motion and data on the forces exerted on the ship along its course and its navigation attitude.

2. The Test Based on a Physical Model

2.1. Equipment

In a generalized water tank with a length of 30 m, a width of 4.5 m, and a height of 1.2 m, a relative static water experiment is conducted to simulate a ship–pier encounter process. The experimental ship model, pier, and sliding platform are shown in Figures 1 and 2. Specifically, a torque sensor is installed on the barycenter of the ship model and connected to a fixed bracket via a rigid rod. The pier model is fixed under the sliding platform vehicle and passes under the ship model at a uniform speed. Along the course, the torque sensor measures the change in the yaw moment (with rotational torque centered on the Z-axis).

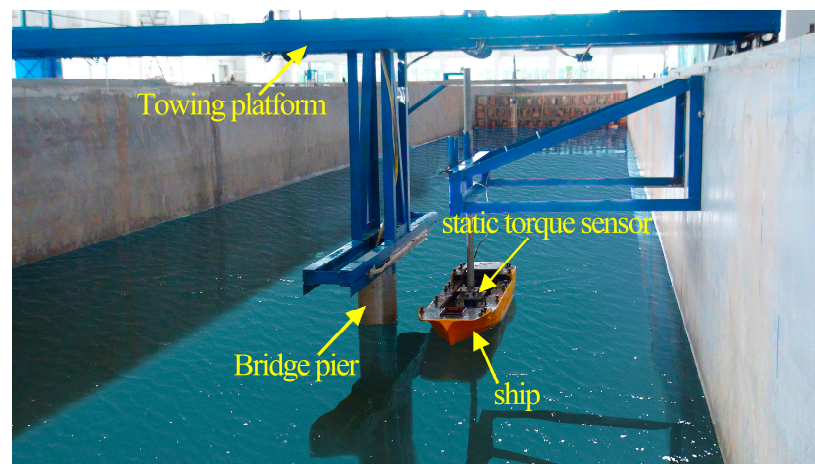


Figure 1. The basin for the ship–pier encounter test.

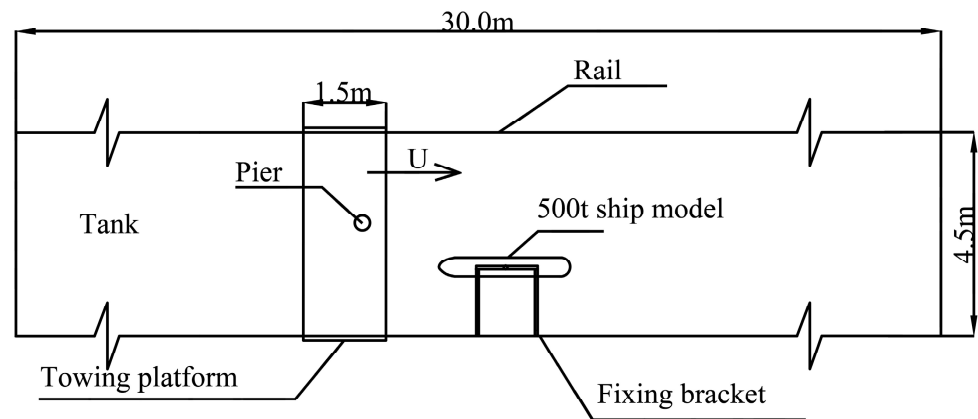


Figure 2. Plan view of ship–bridge intersection test flume.

2.2. Results and Analysis

At a ship–pier transverse distance of $0.9D$, where D represents the pier diameter, the pier moves relative to the ship model at a speed of 0.283 m/s to simulate the change in the yaw moment as the ship passes the pier in the X direction, as shown in Figure 3. It can be seen that the yaw moment demonstrates a “positive peak–negative peak–positive peak” pattern. When the bow approaches the pier, the water between the ship and the pier is squeezed, leading to an increase in the pressure on the side of the bow near the pier. When the bow reaches the center of the pier, the yaw moment reaches the first positive peak; after the flow passes around the pier, a Karman vortex street with periodically shedding vortices is formed behind the pier. Then, as the bow enters the wake flow, it is subject to the attraction or repulsion of the vortex. In this case, for this part of the ship, the flow on the pier side is blocked by the pier and thus has a lower flow speed than that on the other side, while the stern part receives a thrust away from the pier, and the thrust is larger than the force of the wake flow on the ship. Therefore, the yaw moment at this stage is negative and reaches a negative peak as the center of the ship passes the pier; when the stern leaves the pier, the flow channel between the pier and stern increases, and flow rushes in, leading to an increase in the flow speed on the pier side of the stern. With superimposition in the same direction as the negative pressure of the tail vortex, the stern is attracted toward the pier, and the yaw moment reaches its second positive peak. Due to the alternating changes in the tail vortices, the yaw moment fluctuates.

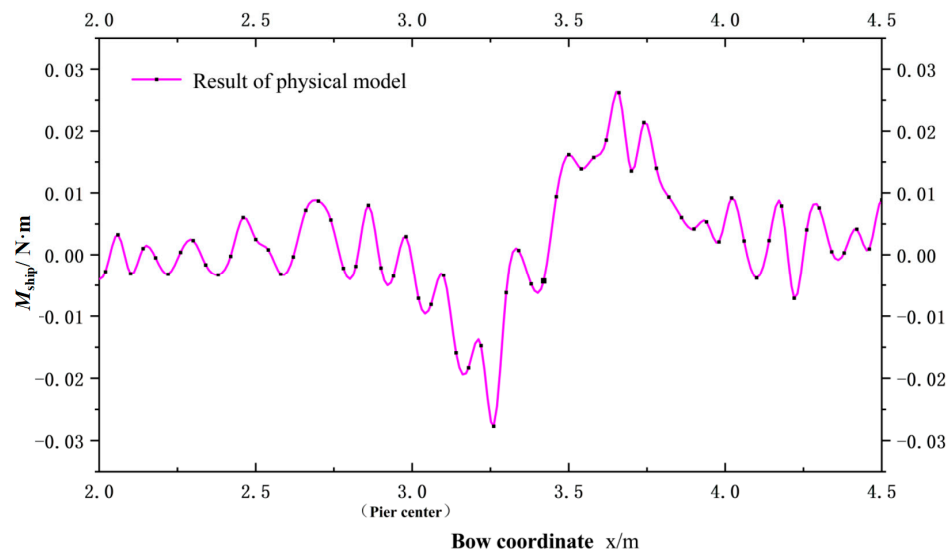


Figure 3. The duration curve of the yaw moment.

3. Numerical Modeling and Verification

With the continuous advancement of CFD, numerical simulation of ship hydrodynamics using the viscous flow method is an efficient and widely used method. This method can eliminate the impact of many disturbing factors, capture the flow field details well, and accurately calculate the forces exerted on a ship. In this study, a numerical simulation of the flow field in the case of a ship–pier encounter was conducted using Fluent, and the simulation results were compared with the yaw moment generated by the corresponding physical model to validate the proposed numerical model.

3.1. Model Size

The geometric scale of the numerical model is 1:50, and a common inland waterway cylindrical pier and a 500 T class barge are selected for the numerical calculation. Herein, the length, width, and draft of the ship are 0.9 m, 0.2 m, and 0.032 m, respectively, and the pier diameter (D) is 0.1 m. As shown in Figure 4, the calculation boundary is set to not disturb the turbulent flow around the pier, the inflow boundary is $55D$ away from the pier axis, the outflow boundary is $45D$ away from the pier axis, and the two symmetric boundaries on both sides are $18D$ and $15D$ away from the pier axis, respectively. The generalized ship model encounters the pier in the X direction at a steady cruising speed v and at a distance of $25D$ from the pier, and the distance between the ship’s side and the pier wall is $T = 16.5D$.

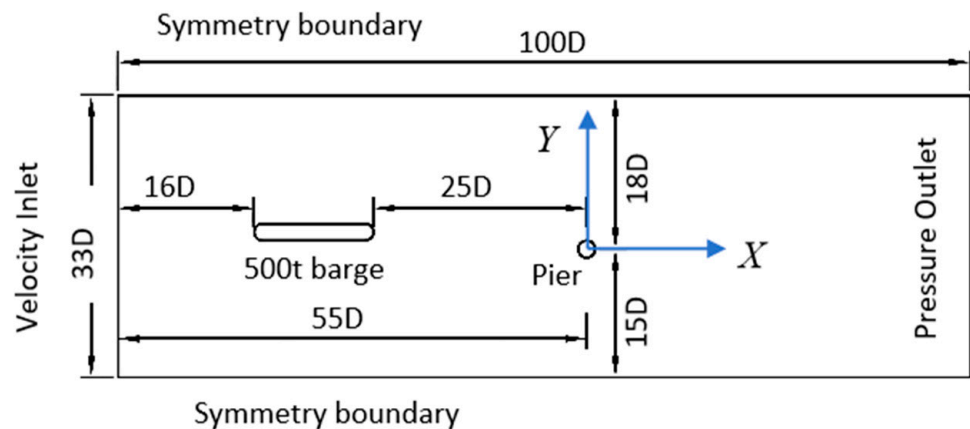


Figure 4. The geometric size of the numerical model.

3.2. The Control Equation

In this study, the numerical calculation first needs to satisfy the two fundamental equations for incompressible viscous fluid, the Navier–Stokes equation and the continuity equation.

The continuity equation for incompressible fluid is as follows:

$$\frac{\partial u_i}{\partial x_i} = 0 \tag{1}$$

The Navier–Stokes equation is as follows:

$$\rho \frac{\partial u_i}{\partial t} + \rho u_j \frac{\partial u_i}{\partial x_j} = -\frac{\partial p}{\partial x_i} + \mu \frac{\partial}{\partial x_j} \left(\frac{\partial u_i}{\partial x_j} \right) \tag{2}$$

The corresponding Reynolds-Averaged Navier–Stokes (RANS) equation can be expressed as

$$\rho \frac{\partial u_i}{\partial t} + \rho u_j \frac{\partial u_i}{\partial x_j} = -\frac{\partial p}{\partial x_i} + \mu \frac{\partial}{\partial x_j} \left(\frac{\partial u_i}{\partial x_j} - \overline{\rho u_i' u_j'} \right) \tag{3}$$

where the values of i and j range from 1 to 3, and u_i, u_j , and p are time-averaged quantities. $-\overline{\rho u_i' u_j'}$ is defined as the Reynolds stress term. The RNG k - ε model is essentially a turbulence model based on the renormalization group (RNG). It is suitable for flows with high strain rates and large streamline curvature and has been widely used for simulations of surface ships. Moreover, the numerical calculation needs to satisfy the transport equations for turbulent kinetic energy and the turbulent dissipation rate.

$$k : \frac{\partial}{\partial t}(\rho k) + \frac{\partial}{\partial x_j}(\rho u_j k) = \rho p - \rho \varepsilon + \frac{\partial}{\partial x_j} \left[\left(\mu + \frac{\mu_t}{\sigma_x} \right) \frac{\partial k}{\partial x_j} \right] \tag{4}$$

$$\varepsilon : \frac{\partial}{\partial t}(\rho \varepsilon) + \frac{\partial}{\partial x_j}(\rho u_j \varepsilon) = C_{\varepsilon 1} f_1 \frac{\rho p \varepsilon}{k} - C_{\varepsilon 2} f_2 \frac{\rho \varepsilon^2}{k} + \frac{\partial}{\partial x_j} \left[\left(\mu + \frac{\mu_t}{\sigma_x} \right) \frac{\partial \varepsilon}{\partial x_j} \right] \tag{5}$$

$$\text{where } \varepsilon = \overline{\frac{\mu}{\rho} \left(\frac{\partial u_i'}{\partial x_k} \right) \left(\frac{\partial u_j'}{\partial x_k} \right)}, \mu_t = \rho C_\mu \frac{k^2}{\varepsilon} \tag{6}$$

where k denotes the turbulent kinetic energy; ε represents the turbulent dissipation rate; u indicates the flow velocity; p denotes the pressure; ρ denotes the density; μ denotes the dynamic viscosity; ν is the dynamic viscosity coefficient; μ_t denotes the turbulent viscosity; and f_1 and f_2 are damping functions. Additionally, $C_\mu = 0.085$, $C_{\varepsilon 1} = 1.42$, $C_{\varepsilon 2} = 1.68$ and $\sigma_\varepsilon = 0.7179$.

3.3. The Numerical Method

3.3.1. Computational Domain Classification and Mesh Generation

In this study, the simplified two-dimensional planar motion of the ship in the bridge area is treated as a three-degrees-of-freedom problem: the longitudinal movement along the X -axis; the lateral drift caused by the transverse forces induced by the disturbed flow around the pier; and the rotation of the ship due to the moment generated by the uneven hydrodynamic distribution. The displacement of the moving ship is significantly larger than the mesh size, which can result in excessive mesh distortion and lead to non-convergence in the calculations. Therefore, the spring smoothing method and the local remeshing method are used to update the mesh. The local remeshing method is only applicable to tetrahedral and triangular meshes, which are unstructured meshes. In the same computational domain, unstructured meshes generate more mesh elements than structured meshes while still satisfying the flow field calculation conditions. To reduce the mesh updating time and save computational resources, a multi-region computational model is employed, as depicted in Figure 5. The interface is used for connection and data transfer between the computational domains. Specifically, Domain 1 contains the ship. It is the dynamic mesh area and uses triangular unstructured meshes. In this domain, quadrilateral meshes are divided around the ship as boundary-layer meshes, which move with the ship, while the other meshes are updated as the ship moves. Domain 2 contains the pier and the other stationary mesh areas. These meshes are not updated as the ship moves, and quadrilateral structured meshes are used. The mesh size has 98,883 cells, and the size of the pier's radial first-layer grid is $0.01D$, also taking a time step size of 0.005 s to calculate. In the preliminary simulation verification, the selected grid density showed consistency with the experimental data and expected results, indicating that the current grid density adequately reflects the actual situation. Therefore, we believe that this grid density is a reasonable choice without increasing the computational burden. Moreover, in critical areas (such as around the ship), more refined boundary-layer meshes (quadrilateral meshes) are used to ensure that the flow details in these areas are fully resolved. This treatment further enhances the overall reliability and accuracy of the simulation.

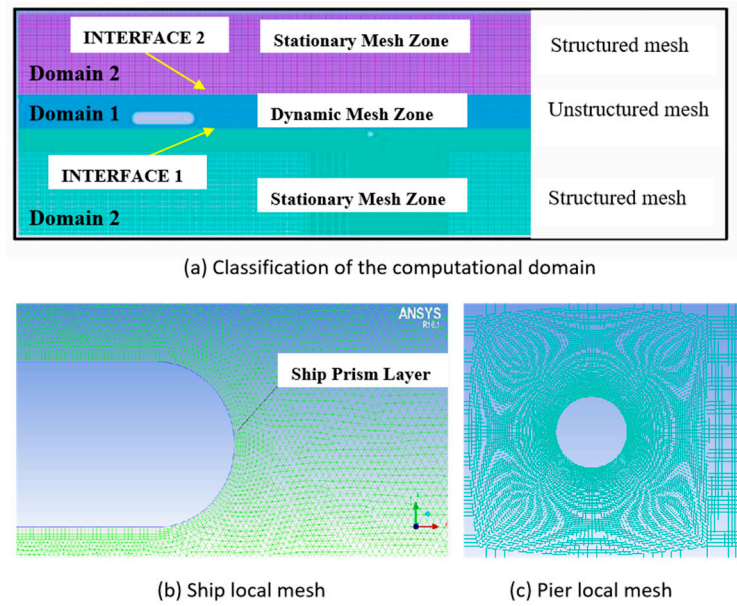


Figure 5. Computational domain classification and mesh generation.

3.3.2. Setting of the Boundary Conditions

Boundary conditions are directly related to the stability and accuracy of numerical calculations. In the model, the inlet boundary is set as a velocity inlet, the outlet boundary is set as a pressure outlet, the two sides are set as symmetrical boundaries, the top is set as an air pressure outlet, the bottom is set as a wall boundary condition, and the pier and ship surfaces are set as walls. The volume of fluid (VOF) function is adopted to construct and track the free fluid surface of the model.

3.3.3. Utilization of the UDF [25]

To simulate the forces exerted on the ship and the motion of the ship under the influence of turbulence around the pier, dynamic meshes are employed to convert forces into velocity and displacement. In this study, the linear speed and the angular speed of the ship at each time step are defined using the dynamic mesh macro “DEFINE_CG_MOTION” in the UDF to specify the ship motion, and the forces exerted on the ship at each time step are obtained using “Compute_Force_And_Moment” to calculate the barycentric speed, angular speed, and barycentric position of the ship at the next time step. In this way, coupling between the flow and ship motion can be obtained.

3.4. Model Verification

3.4.1. Hydrodynamics of the Flow around the Pier

The drag coefficient C_d of the cylindrical pier and the Strouhal number, which indicates the shedding frequency of the tail vortices, are calculated by using the mathematic model of the flows around the 2D cylinder without the ship’s interference. using Formulas (7) and (8) to compute the drag coefficient and the Strouhal number, the results are compared with experimental values with similar Reynolds numbers. The average drag coefficient calculated for the flow around a single pier is $C_d = 1.182$, and the Strouhal number is $s_t = 0.201$, which are close to the experimental values found for the single-pier model by Yokuda and Ramaprian [26] ($C_d = 1.20, s_t = 0.21$).

$$C_d = \frac{2F}{\rho U^2 D} \tag{7}$$

$$S_t = \frac{fD}{U} \tag{8}$$

where F is the resistance, U is the incoming flow velocity, D is the pier diameter, and ρ denotes the density. f is the vortex separation frequency.

3.4.2. The Flow Field of the Flow around the Pier

PIV enables transient, non-contact testing of the flow field. To obtain a fine-grained analysis of the flow field behind the pier, this study uses PIV in a $16\text{ m} \times 0.4\text{ m} \times 0.5\text{ m}$ glass water tank to observe the flow field behind the pier. Through the experiment using the PIV physical model, the numerical simulation results at a flow velocity of 2.0 m/s and the surface flow field around the pier are shown in Figure 6a and Figure 6b, respectively. It can be seen that the streamline directions, vortex directions, and vortex-shedding patterns of the tail wake behind the pier in the numerical model are consistent with the observations from the physical model.

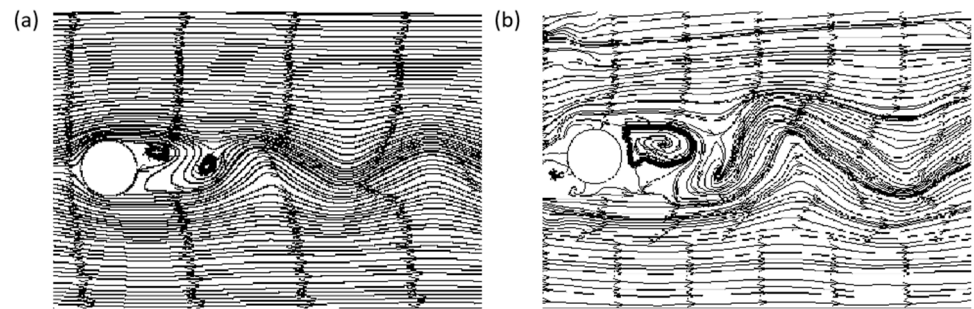


Figure 6. (a) The streamline distribution behind the pier in the numerical model. (b) The streamline distribution behind the pier in the physical model of PIV.

3.4.3. Verification of the Force Exerted on the Ship

The numerical model corresponding to the physical model was calculated in the following conditions: $T = 0.9D$ and the ship passing the pier in the X direction at a speed of 0.283 m/s . As illustrated in Figure 7, the yaw moment generated by the physical model and the numerical calculation demonstrates consistent patterns (positive peak–negative peak–positive peak).

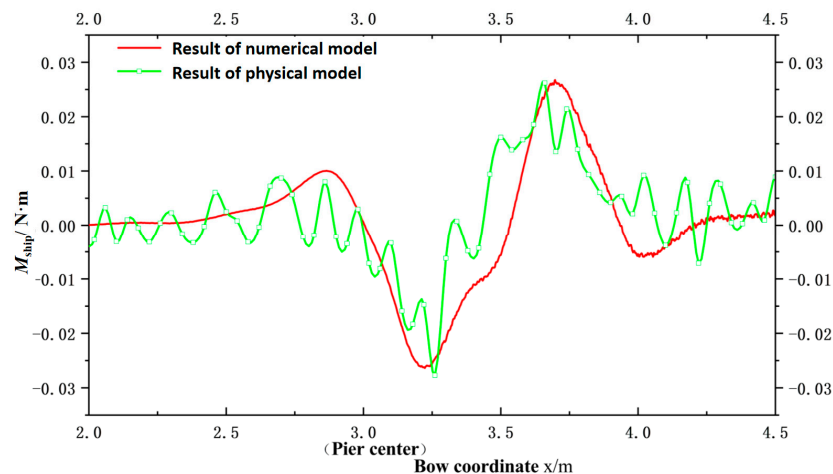


Figure 7. The duration curves of the yaw moment.

Although the high-frequency oscillations and wake diffusion present in the experiment were not simulated, the flow field calculation results in the simulation model are consistent with the flow field structure of the flow around the pier. Specifically, the hydraulic characteristics are comparable, the change patterns for the ship’s yaw moment are consistent, and reasonable numerical solutions are acquired. Therefore, the meshes and

the numerical method in this numerical model can meet the requirements for numerical calculations and are suitable for simulating the ship–pier encounter process.

4. Numerical Calculation Results and Analysis

4.1. Determination of the Calculation Conditions

Considering the common flow velocity during the flood season in the Xiangjiang River, the flow velocity in front of the bridge is set to 0.283 m/s (perpendicular to the bridge axis). This study aims to investigate the pattern of the forces exerted on ships caused by the flow around piers without considering the effects of steering and ship waves. Therefore, a relatively low speed against the bank is chosen for the study. Herein, the ship speed against the bank is set to 0.566 m/s. Based on these parameter settings and considering different ship–pier transverse distances (0.6D, 0.9D, 1.2D, and 1.5D), the coupling between the ship and the turbulence around the pier when the ship passes the pier in the X direction are analyzed.

4.2. Effects of the Ship–Pier Transverse Distance on the Force Exerted on the Ship and the Motion of the Ship

4.2.1. Force Analysis

When the ship passes piers at different ship–pier transverse distances, the duration curves of the lateral force exerted on the ship (causing the ship to move laterally along the Y axis) and the yaw moment of the ship are demonstrated in Figure 8a and Figure 8b, respectively.

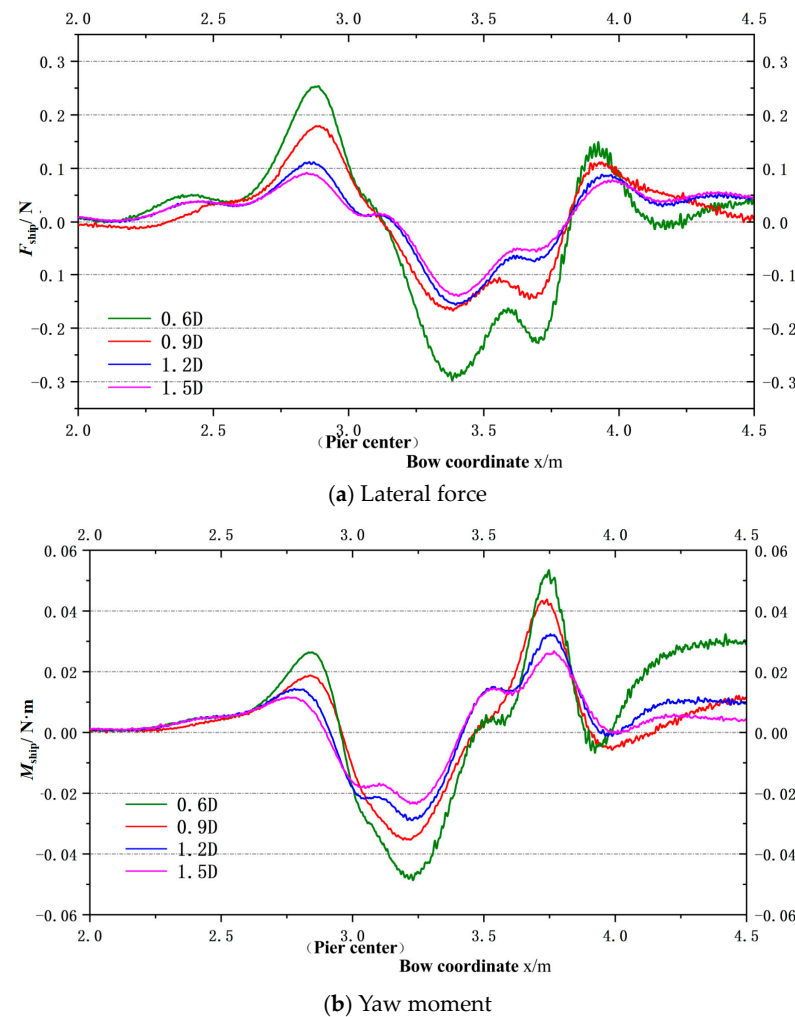


Figure 8. The duration curves at different transverse distances.

Since the lateral force is the root cause of the yaw moment, they are consistent. It can be seen that at different transverse distances, the evolution patterns of the lateral force and the yaw moment are almost the same (see Section 2.2), and transverse distance has little effect on the timing of the positive lateral force and the positive yaw moments of the ship. For the positive lateral forces exerted on the ship at different transverse distances (see Table 1), the maximum negative peak is about 0.287 N when $T = 0.6D$, which can generate a transient acceleration of 0.087 m/s^2 for a 500 T class barge model, pushing the ship laterally to approach the pier. As the ship–bridge distance increases, both the positive and negative peaks of the lateral force exerted on the ship and the yaw moment of the ship decrease, and the rate of this decrease diminishes, indicating that the disturbance effect of the pier and the tail vortices behind the pier on the ship weakens as the ship–bridge distance increases.

Table 1. The peak lateral force, acceleration, and peak yaw moment of the ship at different values of T .

T	$F_{y\max}$ (N)	a (m/s^2)	M^+_{\max} (N·m)	M^-_{\max} (N·m)
$0.6D$	−0.287	0.0718	0.0509	−0.0472
$0.9D$	0.167	0.0417	0.0402	−0.0358
$1.2D$	−0.156	0.0583	0.0319	−0.0289
$1.5D$	−0.140	0.0503	0.0263	−0.0229

To better explain the evolution of the yaw moment ($T = 0.6D$), a comprehensive analysis is conducted. This analysis combines the lateral velocity distribution around the pier with local streamlines and the pressure distribution around the ship at typical positions as it passes the pier, as shown in Figure 9.

As shown in Figure 9b, when the ship approaches the pier, the flow at the right front end of the ship moves diagonally towards the pier. At the same time, the proximity of the ship’s boundary somewhat suppresses the development of streamlines around the stagnation point in front of the pier. The water between the ship and the pier is continuously compressed, and together with the pushing flow in front of the pier, this causes the pressure at the right bow of the ship to be greater than that at the left bow. As a result, the bow is repelled away from the pier, changing the ship’s heading. When the bow is about to reach the pier, the channel between the ship and the pier is at its narrowest, the repulsive force is at its maximum, and the yaw moment reaches a positive peak. When the bow enters the wake region of the pier and the stern is still upstream of the pier, as shown in Figure 9c, the upstream boundary of the ship continues to compress the water between the ship and the pier. The right side of the ship’s bow experiences positive pressure, pushing it away from the pier. The flow carried by the bow accelerates out of the channel between the ship and the pier, causing it to spread out behind the pier, enhancing the development of the wake vortex. This increases the negative pressure area behind the pier compared to when no ship is present. The right side of the ship’s stern, located downstream of the pier, is subject to negative pressure, drawing the bow towards the pier. Since the right side of the ship’s bow is attracted while the stern is repelled, a clockwise moment is created, resulting in a negative yaw moment. At this point, if the bow is sucked into the wake region, the ship can easily lose control and collide with the pier. As the stern moves away from the pier, parts of the wake vortex either strike the ship or attach to it, or they mix more intensely with the surrounding vortices. Additionally, the flow carried by the stern accelerates the water in the channel between the stern and the pier, making the negative pressure region behind the pier more pronounced. As shown in Figure 9d, the right side of the stern is within the negative pressure area, indicating that the second positive peak of the yaw moment is mainly due to the negative pressure of the vortex. Because the stern is attracted, there is a risk of the stern swinging into the pier at this point.

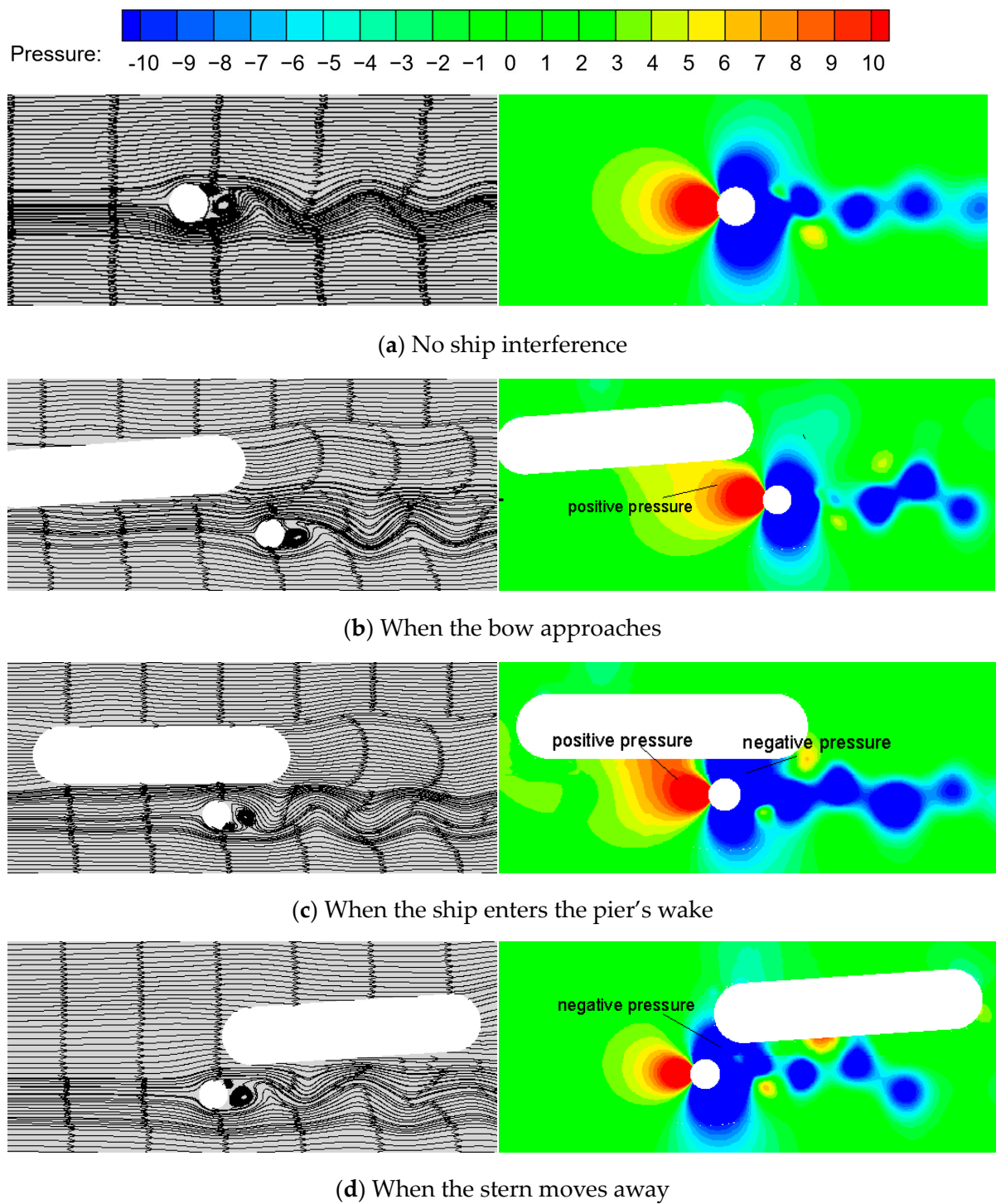


Figure 9. Local streamline and pressure distribution diagrams at typical positions during the ship–pier interaction.

4.2.2. The Barycentric Displacement of the Ship

Figure 10 illustrates the change curve for the Y barycentric coordinate of the ship when it passes the pier when $T = 0.6D$, $0.9D$, $1.2D$, and $1.5D$. It is observed that the ship's barycenter slightly approaches the pier before moving away at distances of $0.6D$, $0.9D$, $1.2D$, and $1.5D$. When $T = 0.6D$ and $0.9D$, the ship approaches and moves away from the pier at larger magnitudes; when $T = 1.2D$ and $1.5D$, the Y barycentric coordinate of the ship remains almost unchanged.

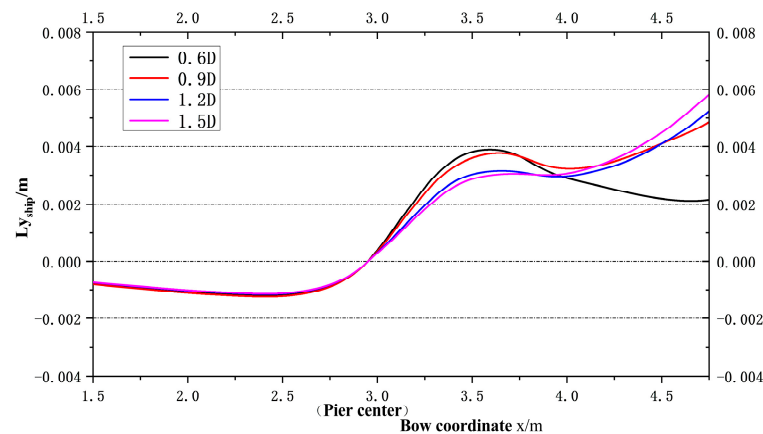


Figure 10. The ship displacement according to the Y barycentric coordinate and a diagram of the ship's position.

When $T = 0.6D$, the ship travels in the X direction at a certain speed (without steering control). When the bow approaches the pier, the positive yaw moment gradually increases. This is reflected in the fact that the bow is deflected away from the pier side, and the stern is deflected towards the pier side, i.e., it is deflected counterclockwise, and the barycenter approaches the pier. As the ship continues to travel in the X direction, the yaw moment becomes negative, the bow is attracted by the negative pressure on the pier side and the tail of the pier, and the stern is repelled, deflecting clockwise overall. After the ship passes the pier, the barycenter still tends to approach the pier side due to inertia and the push of the incoming flow, leading to a peak in the lateral offset of the ship's barycentric; as the ship continues to travel in this direction, the yaw moment becomes positive again and reaches its maximum when the stern is at the pier position, the trend in the ship's barycentric position approaching the pier gradually flattens, and the ship tends to move laterally away from the pier. When $T = 0.9D$, $1.2D$, and $1.5D$, the pattern of the change in the yaw moment of the ship along the course is essentially the same as that at $0.6D$, and as the ship-pier transverse distance increases, the positive lateral force and the positive yaw moment along the course decrease, and thus the peak of the barycentric lateral offset also decreases. After the stern passes the pier, the yaw moment becomes positive, deflecting the ship counterclockwise, and the barycenter quickly moves away from the pier. Therefore, when $T = 0.6D$, after the ship is affected by the hydrodynamic disturbance of the pier, the barycentric lateral offset becomes large, and when the stern passes the pier, there is a high risk that the ship rear collides with the bridge and the stern hits the pier. When the transverse distance is greater than $0.9D$, after the stern passes the pier, the transverse distance between the barycentric position and the pier significantly increases, indicating a small chance of the stern hitting the pier, i.e., the adverse effect of the pier on the navigation of the ship is small.

5. Conclusions

This study analyzes the change patterns for the lateral force, yaw moment, and barycentric displacement of a ship at different ship-pier transverse distances in a ship-pier encounter process. The proposed numerical simulation method can reasonably predict the forces exerted on the ship and the motion of the ship passing a pier under the impact of the turbulent flow. The lateral force and the yaw moment exerted on the ship passing through the pier at different ship-pier transverse distances are affected by the pier and tail vortices behind the pier, and their duration curves show repetitive fluctuations with distinct peaks (i.e., a positive peak, a negative peak, and a positive peak). When the bow reaches the center of the pier, the ship is subject to repulsion, which causes the yaw moment to reach a positive peak (counterclockwise); meanwhile, the barycenter of the ship first moves laterally closer and then away from the pier, while the stern turns towards the pier; after the center of the ship passes the pier, the ship passes the pier with the bow inward (closer to the pier side)

and the stern outward (away from the pier side), and the lateral force reaches a negative peak, which generates lateral acceleration that brings the ship closer to the pier; when the stern is about to leave the pier, the yaw moment reaches a positive peak, and the stern turns towards the pier again. Through a sensitivity analysis of the influence of the ship–pier transverse distance on the unsteady hydrodynamics of the ship passing the pier, it is found that as the ship–pier transverse distance increases, the maximum positive and negative peaks of the lateral force and the yaw moment decrease. At ship–pier distances of $0.9D$, $1.2D$, and $1.5D$, both the lateral force and the yaw moment are minimal. Additionally, the trajectories of the ship’s barycenter as it passes the pier are similar, exhibiting only minor variations with the change of distances. After the stern passes the pier, the ship quickly moves laterally away from the pier, and the pier has little impact on the ship’s navigation in this process. Therefore, $0.9D$ can be considered a safe reference distance between ships and piers near a bridge. This study uses a two-dimensional numerical model, only considering the motion at three degrees of freedom of the ship. In future work, three-dimensional numerical calculations could be considered to fully account for the ship’s six degrees of freedom. Additionally, rudder forces could be included in the UDF to make the numerical model more realistic.

Author Contributions: Conceptualization, Y.Y. (Yasi Ye) and X.L.; methodology, Y.Y. (Yasi Ye); formal analysis, Y.Y. (Yukang Ye); writing—original draft preparation, Y.Y. (Yasi Ye), A.L., J.Z. and Q.R. All authors have read and agreed to the published version of the manuscript.

Funding: This research received no external funding.

Institutional Review Board Statement: Not applicable.

Informed Consent Statement: Not applicable.

Data Availability Statement: Data are contained within the article.

Conflicts of Interest: Authors Yasi Ye and Qijiang Ren were employed by the company Hunan Provincial Communications Planning Survey & Design Institute. The remaining authors declare that the research was conducted in the absence of any commercial or financial relationships that could be construed as a potential conflict of interest.

References

1. Liu, J.; Li, Z.; Huang, H.; Lin, W.; Sun, Z.; Chen, F. Three-dimensional turbulent simulation of bivariate normal distribution protection device. *J. Mar. Sci. Eng.* **2024**, *12*, 602. [\[CrossRef\]](#)
2. Li, J.; Yang, Y.; Yang, Z. Influence of scour development on turbulent flow field in front of a bridge pier. *Water* **2020**, *12*, 2370. [\[CrossRef\]](#)
3. Singh, N.B.; Devi, T.T.; Kumar, B. The local scour around bridge piers—a review of remedial techniques. *ISH J. Hydraul. Eng.* **2022**, *28* (Suppl. 1), 527–540. [\[CrossRef\]](#)
4. Geng, Y.; Guo, M.; Guo, H.; Chen, H. Safety range in bridge areas based on the influence of cross flow on ship navigation. *Ocean Eng.* **2023**, *281*, 114649. [\[CrossRef\]](#)
5. Du, P.; Ouahsine, A.; Sergent, P.; Hoarau, Y.; Hu, H. Investigation on resistance, squat and ship-generated waves of inland convoy passing bridge piers in a confined waterway. *J. Mar. Sci. Eng.* **2021**, *9*, 1125. [\[CrossRef\]](#)
6. Liu, X.P.; Qian, D.Y.; Fang, S.S.; Zhang, Y. Study on the width of turbulent area around pier with ship impact. *Appl. Mech. Mater.* **2012**, *137*, 186–191. [\[CrossRef\]](#)
7. Li, A.; Zhang, G.; Liu, X.; Yu, Y.; Zhang, X.; Ma, H.; Zhang, J. Hydrodynamic characteristics at intersection areas of ship and bridge pier with skew bridge. *Water* **2022**, *14*, 904. [\[CrossRef\]](#)
8. Wnek, A.D.; Sutulo, S.; Guedes Soares, C. CFD analysis of ship-to-ship hydrodynamic interaction. *J. Mar. Sci. Appl.* **2018**, *17*, 21–37. [\[CrossRef\]](#)
9. Woolliscroft, M.O.; Maki, K.J. A fast-running CFD formulation for unsteady ship maneuvering performance prediction. *Ocean Eng.* **2016**, *117*, 154–162. [\[CrossRef\]](#)
10. Stern, F.; Yang, J.; Wang, Z.; Sadat-Hosseini, H.; Mousaviraad, M.; Bhushan, S.; Xing, T. Computational ship hydrodynamics: Nowadays and way forward. *Int. Shipbuild. Prog.* **2013**, *60*, 3–105.
11. Zhou, J.; Ren, J.; Bai, W. Survey on hydrodynamic analysis of ship–ship interaction during the past decade. *Ocean Eng.* **2023**, *278*, 114361. [\[CrossRef\]](#)
12. Tuck, E.O.; Newman, J.N. Hydrodynamic interactions between ships. In Proceedings of the 10th ONR Symposium on Naval Hydrodynamics, Cambridge, MA, USA, 24–28 June 1974.

13. Kijima, K. Prediction method for ship manoeuvring motion in the proximity of a pier. *Ship Technol. Res.* **1997**, *44*, 22–31.
14. Arslan, T.; Pettersen, B.; Andersson, H.I. Investigation of the flow around two interacting ship-like sections. *J. Fluids Eng.* **2015**, *137*, 041205. [[CrossRef](#)]
15. Nam, B.W.; Kim, Y.; Hong, S.Y. Hydrodynamic interaction between two barges during berthing operation in regular waves. *Ocean Eng.* **2015**, *106*, 317–328. [[CrossRef](#)]
16. Xu, Y.; Liu, M. Study on critical hydrodynamics interaction of incontrollable status in pier waters. *Transp. Sci. Technol.* **2008**, *3*, 103–106.
17. Gan, L.; Zou, Z.; Xu, H. Calculation and analysis of the hydrodynamic forces on a ship navigating in bridge area. *J. Ship Mech.* **2014**, *6*, 613–622.
18. Sutulo, S.; Soares, C.G.; Otzen, J.F. Validation of potential-flow estimation of interaction forces acting upon ship hulls in parallel motion. *J. Ship Res.* **2012**, *56*, 129–145. [[CrossRef](#)]
19. Pinkster, J.A. Progress on real-time prediction of ship-ship-shore interactions based on potential flow. In Proceedings of the 4th MASHCON: International Conference on Ship Manoeuvring in Shallow and Confined Water, Hamburg, Germany, 23–25 May 2016; pp. 23–25.
20. Ye, X.; Fan, W.; Sha, Y.; Hua, X.; Wu, Q.; Ren, Y. Fluid-structure interaction analysis of oblique ship-bridge collisions. *Eng. Struct.* **2023**, *274*, 115129. [[CrossRef](#)]
21. Eloot, K.; Vantorre, M. Ship behaviour in shallow and confined water: An overview of hydrodynamic effects through EFD. In *Assessment of Stability and Control Prediction Methods for NATO Air and Sea Vehicles*; Research and Technology Organisation (RTO): Portsmouth, UK, 2011; p. 20.
22. Beck, R.F. Hydrodynamic forces caused by a ship in confined waters. *J. Eng. Mech. Div.* **1981**, *107*, 523–546. [[CrossRef](#)]
23. Huang, J.; Xu, C.; Xin, P.; Zhou, X.; Sutulo, S.; Soares, C.G. A fast algorithm for the prediction of ship-bank interaction in shallow water. *J. Mar. Sci. Eng.* **2020**, *8*, 927. [[CrossRef](#)]
24. Nandhini, V.; Nallayarasu, S. CFD simulation of the passing vessel effects on moored vessel. *Ships Offshore Struct.* **2020**, *15*, 184–199. [[CrossRef](#)]
25. ANSYS Inc. *ANSYS Fluent User's Guide 13.0. [Manual]*; ANSYS Inc.: Canonsburg, PA, USA, 2009.
26. Yokuda, S.; Ramapriam, B.R. The dynamics of flow around a cylinder at subcritical Reynolds numbers. *Physic Fluids* **1990**, *2*, 784–791. [[CrossRef](#)]

Disclaimer/Publisher's Note: The statements, opinions and data contained in all publications are solely those of the individual author(s) and contributor(s) and not of MDPI and/or the editor(s). MDPI and/or the editor(s) disclaim responsibility for any injury to people or property resulting from any ideas, methods, instructions or products referred to in the content.